PROGRESS REPORT

ON

"DEVELOPMENT OF NOVEL COMPOSITE AND RANDOM MATERIALS FOR NONLINEAR OPTICS AND LASERS"

NASA GRANT#: NCC-1-01049

FOR PERIOD

SEPTEMBER 15, 2001 – SEPTEMBER 14, 2002

SUBMITTED BY:

DR. MIKHAIL NOGINOV
CENTER FOR MATERIALS RESEARCH
NORFOLK STATE UNIVERSITY
NORFOLK, VA 23504

CONTENTS page #

1 TECHNICAL REPORT

1.1 Formation of a coherent mode in solid-state random laser

Abstract

A qualitative model explaining sharp spectral peaks in emission of solid-state random laser mateials with broad-band gain is proposed. The suggested mechanism of coherent emission relies on synchronization of phases in an ensemble of emitting centers, via time delays provided by a network of random scatterers, and amplification of spontaneous emission that supports the spontaneously organized coherent state.

Laser-like emission from powders of solid-state luminophosphors, characterized by dramatic narrowing of the emission spectrum and shortening of emission pulses above the threshold, was first observed by Markushev *et al.* [1.1] and further studied by a number of research groups [1.2-1.6]. In particular, it has been shown that when the pumping energy significantly exceeds the threshold, one or several narrow emission lines can be observed in broad-band gain media with scatterers, such as films of ZnO nanoparticles [1.4,1.7-1.11], films of π-conjugated polymers [1.12,1.6], or infiltrated opals [1.13,1.6].

The experimental features, commonly observed in various solid-state random laser materials characterized by different particle sizes, different values of the photon mean free path l^*, different indexes of refraction, *etc.* [1.4,1.6,1.7-1.13], can be described as follows. (Liquid dye random lasers [1.14] are not discussed here.)

At weak pumping, only spontaneous emission is observed. The spatial uniformity of luminescence emerging from the surface of the sample resembles that of pumping.

At more intense pumping, amplified spontaneous emission (ASE) is getting strong, causing narrowing of the emission spectrum.

When pumping power reaches the threshold, the first narrow emission peak appears in the spectrum close to the top of the ASE band. The spectral width of this peak can be several tens times smaller than that of the ASE band. Simultaneously, first bright spots appear in the in the near-field emission pattern [1.9,1.10]. (Similar spatial confinement of stimulated emission above the threshold was first observed in powders of Nd^{3+}-containing materials [1.15,1.16]. Gain bands of rare-earth (RE) ions are typically narrow. Probably that is why observations of multiple-line random laser emission in RE-containing materials are rare [1.17,1.18,1.3].)

At the further increase of the pumping power, the number of sharp peaks in the spectrum and the number of bright spots in the near field emission increase. The transformation of the emission spectrum in ZnO powder with the increase of the pumping power is shown in Figure 1.1.

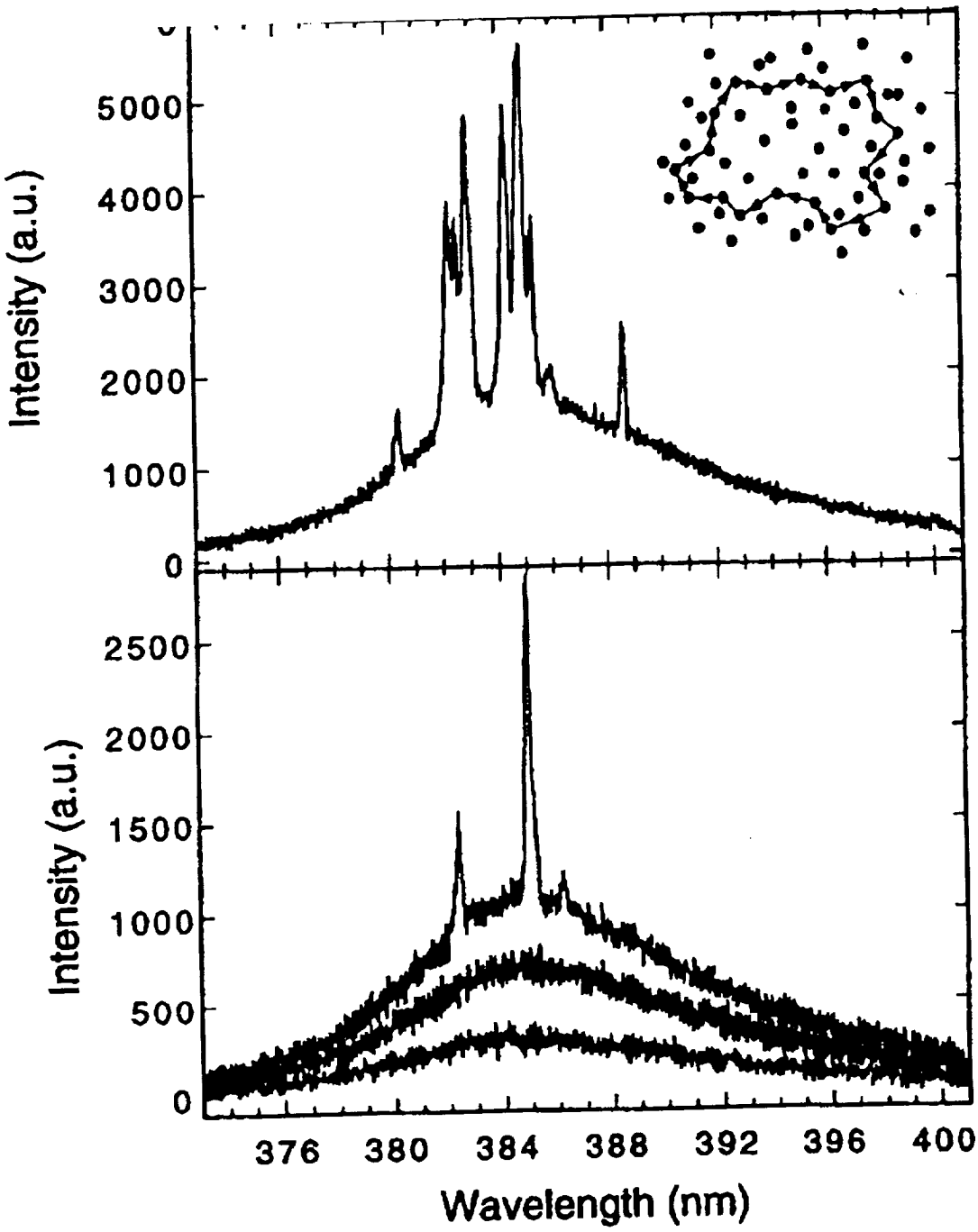

Figure 1.1. Transformation of the emission spectrum in ZnO powder with increase of the pumping intensity (from bottom to top) 400, 562, 763, 875, and 1387 kW/cm^2. Inset – schematic diagram of the closed loop path. (Adopted from Ref. [1.8].)

The spectral positions of the narrow emission peaks are specific to the particular pumped spot. When the pumping beam is moved along the surface of the sample, the wavelengths of the emission lines change randomly. Qualitatively, this behavior is similar to that on a more conventional laser with optically clear gain medium and highly scattering ("speckle") back mirror [1.19].

To explain the experimental results above, Cao et al. suggested that because of very strong scattering in ZnO powder, the closed-loop paths, which serve as ring laser cavities, can be formed in a random medium through multiple optical scattering [1.4,1.8] (Figure 1.1, inset). Accordingly, narrow lines observed in the random laser emission are the modes of the ring cavities. Although this simple model qualitatively explains some of the experimental effects, it fails at more detailed examination. For example, in Ref. [1.8], in order to determine the minimum size of the closed-loop path, the area of the pumping spot S was changed, while the pumping density was kept constant. It was found that at some particular pumping density, no sharp peaks appeared in the spectrum at S=980 μm^2, and the conclusion was made that the minimum loop was larger than this area. At the same time, five narrow peaks were observed at S=1350 μm^2 and more than twelve peaks were observed at S=1870 μm^2. According to Refs. [1.9,1.10], bright spots in near-field emission co-exist next to each other and typically do not overlap much, especially close to the laser threshold. Thus, it appears strange that more than twelve loops can fit 1870 μm^2 spot if one loop cannot fit 980 μm^2 spot.

Additionally, to provide for a reasonably high quality factor of the cavity, the loop model should assume specular reflections off scatterers. This is difficult to

imagine in the case when the average size of ZnO particles, d≈0.1μm, is much smaller than the emission wavelength, λ≈0.4 μm. When the length of the loop L (which can be estimated as $L\approx\sqrt{S}$>31 μm) is much larger than the square root of the scattering cross section $\sqrt{\sigma}$ (which is probably not larger than the maximum of d and λ), the loss in the cavity should be extremely large. At isotropic scattering, the output coupling of such cavity can be estimated as O.C.$\approx 1-\sigma/4\pi L^2=1-\lambda^2/4\pi L^2\approx$0.99999 (or 99.999%), which makes the cavity essentially nonexistent.

The Fourier transform of the stimulated emission spectrum in π-conjugated polymeric film was done in Refs. [1.6,1.12]. Based on the assumptions of a simple closed-loop model, it was determined that the loops in the sample had two sizes, $15l^*$ and $18l^*$, where l^* was equal to 15 μm [1.12]. The analysis of the experimental parameters in Ref. [1.12] (not shown here for brevity) suggested that the number of loops contributing to the recorded emission spectrum was large, $\approx 10^2$. It is rather unclear why all $\approx 10^2$ loops had only two sizes, $15l^*$ and $18l^*$. Why there were no loops of other sizes? Actual photon free paths are shorter and longer than l^*. This implies that the distribution of the loop lengths should be almost continuous and the Fourier transform of the experimental spectrum should be smeared out. However, this did not happen. All the discrepancies above suggest that the simple closed-loop model is not adequate enough.

As it has been pointed out in Ref. [1.10], no sharp peaks in the spectrum and bright spots in the near-field emission pattern can be predicted if the phase of the optical field is neglected [1.20-1.23]. In Refs. [1.10,1.11,1.24], the electromagnetic field distribution was calculated in random medium by solving Maxwell equations

along with rate equations for excited electronic states. A reasonably good agreement between calculation and experiment has been demonstrated [1.10,1.24]. However, numerical simulations do not help to understand the underlying physical processes.

In this work, we propose a qualitative model explaining self-organization of a coherent stimulated emission state in random lasers from a chaotic distribution of spontaneously emitted photons with individual random frequencies and phases.

Let us first consider a hypothetical collection of randomly positioned point sources of monochromatic light, all of which have random phases, Figure 1.2a. [In random lasers, one can reach the monochromaticity high enough, such that the longitudinal coherence length l_c ($\approx$1cm [1.25]) will be much larger than the size of the medium.] In principle, one can insert in the medium a number of time delay devices (slabs, prisms, reflectors, etc.) and, with the use of these devices, synchronize phases in certain (larger or smaller) ensembles of light sources, Figure 1.2b. In other terms, an interference pattern can be formed in the medium, such that the light sources belonging to selected ensembles will be positioned in hot spots of the light distribution pattern.

Certainly, any given configuration of time delay devices, which provide phase synchronization within an ensemble, is wavelength-specific. If the emission wavelength is changed slightly, all time delays have to be adjusted to keep synchronization. However, it is also possible that the same configuration of time delay devices can support a number of discrete frequencies, like common laser resonators do.

If the point sources are atoms or clusters of atoms excited to the state of population inversion, then synchronized radiation, projected from one point source to another, will induce stimulated emission, which will support the existing interference pattern and enhance the "mode" of radiation. Obviously, the sharper

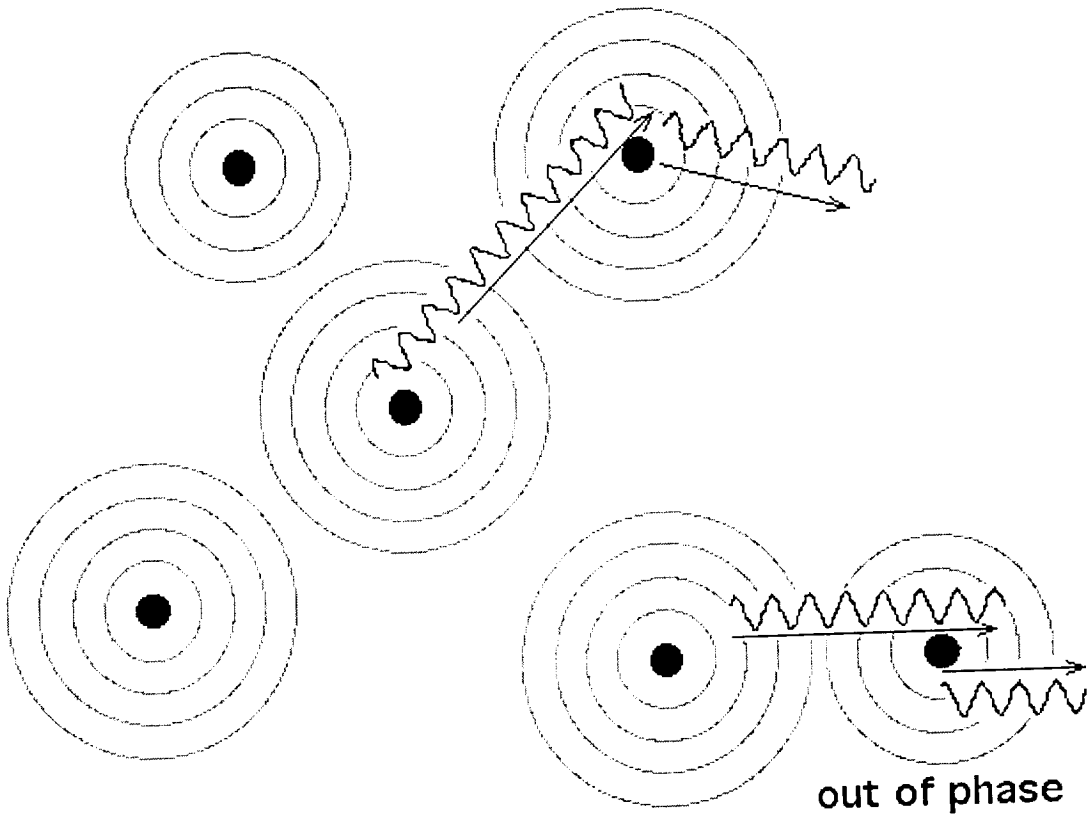

Figure 1.2a. Point sources of monochromatic light emitting with random phases.

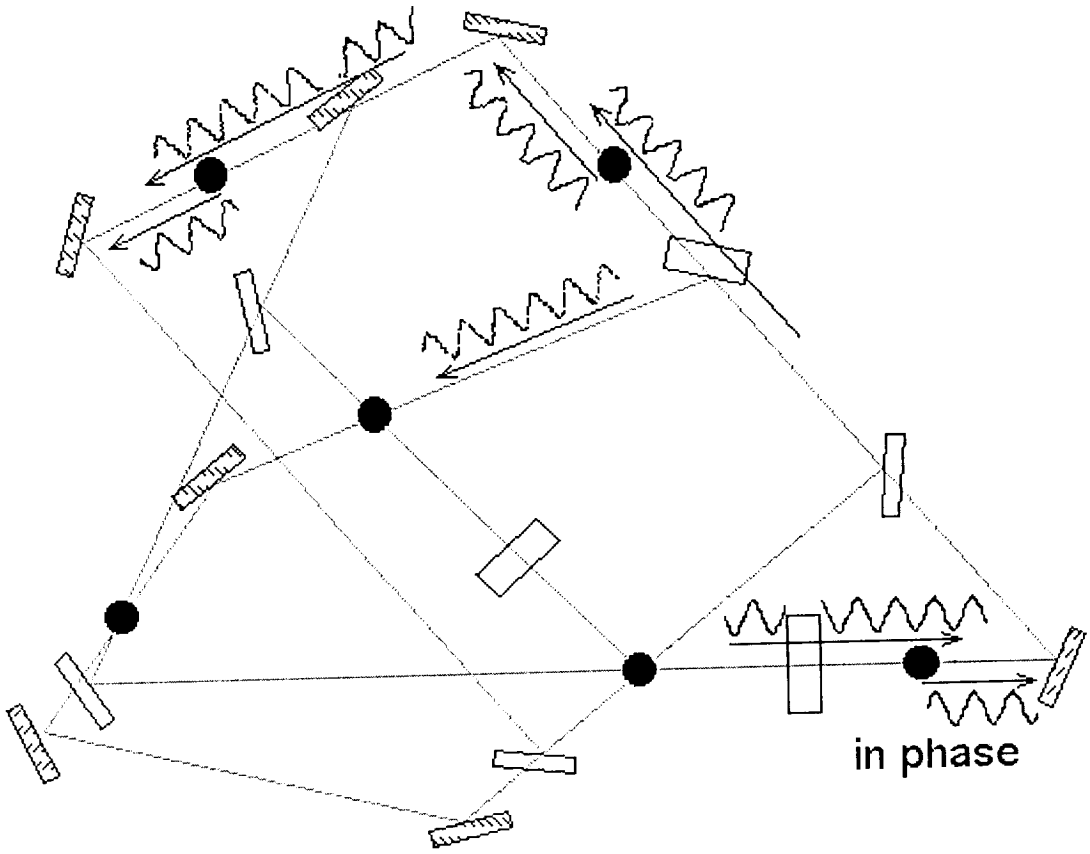

Figure 1.2b. Ensemble of the same point sources as in Figure 2a, along with time-delaying devices (shown as rectangular blocks) which synchronize radiation phases, providing for a formation of complex coherent electromagnetic mode.

the contrast of the interference pattern and the better the spatial overlap of its hot spots and the emitting centers, the more efficient the stimulated emission is.

Typical solid-state random laser material is a dielectric or semiconductor powder or ceramic. It has active gain medium inside microcrystallines, air gaps between particles, and random scatterers (microcrystallines and their surfaces). (With little modification, the discussion below can also be applied to scattering polymers). Under weak optical pumping, active medium emits spontaneous

radiation. If the spectral band of the luminescence transition is broad, then the spectral density of spontaneous emission is low. The photons, of cause, are emitted in different (random) directions and the corresponding waves have different (random) phases. At some instants, certain ("lucky") ensembles of emitting atoms are realized, when randomly walking photons go through a right combination of scatterers, such that atoms illuminate each other with synchronized radiation, Figure 1.2b. The probability of such events is low. Besides, because of low gain, spontaneously emitted photons cannot induce sufficient number of stimulated transitions to support the mode. Thus, instant coherent configurations randomly created from chaotic field distribution momentarily vanish.

A stronger pumping leads to more efficient ASE and corresponding narrowing of the emission line. Thus, the spectral density of the emitted photons is getting higher. This makes the realization of a synchronized mode more probable. What is more important, when the coherent state (synchronized mode) actualizes, it has high probability of getting amplified *via* stimulated emission and becoming self-sustained. It appears likely that during some initial period of time the mode self-adjusts its shape and phase, increasing the contrast of interference pattern and the efficiency of stimulated emission.

Although both "photons" and "waves" were used in the discussion above, the formation of a spatially distributed coherent state is easier to understand in terms of waves and interfering electromagnetic fields. Similarly to the case of conventional lasers, the formation of a coherent mode in random lasers is difficult to explain in terms of photons as particles.

As it logically follows from the discussion above, the appearance of the synchronized mode should lead to the emergence of a narrow peak in the emission spectrum and to the onset of more efficient stimulated emission in the ensemble of coherently coupled (by radiation) excited atoms or ions. Thus, the model explains both sharp peaks in the spectrum and bright spots in the near-field emission observed in many experimental works. The pumping power corresponding to the onset of the highly intense coherent emission state can be defined as the random laser threshold. This definition is not in disagreement with that suggested by Letokhov [1.26], who using the analogy with nuclear fusion, suggested that at the random laser threshold, the number of photons generated in a gain volume should increase the number of photons leaving the same volume per unit time. The same criterion applies to the present model. What has not been taken into account in Ref. [1.26] is the formation of the *coherent* emission state and the interference pattern which effectively enhance the stimulated emission.

In the proposed model, the wavelength of the narrow stimulated emission line is strongly dependent on the particular configuration of the ensemble of scatterers. Thus, when the pumping beam is moved along the sample surface and different subvolumes containing emitting sources and scatterers are excited, the wavelength of emission should change in the vicinity of flat top of a broad gain spectrum. This behavior has been observed experimentally.

With an increase of pumping power, self-assembling of stimulated emission in other ensembles, with less fortunate configuration of scatterers, can emerge,

leading to the appearance of other narrow peaks in the spectrum and bright spots in the near field pattern, again, in accord with experimental observations.

Several questions relevant to the discussion above arise.

(1) How sharp is the contrast of the interference pattern and how the distribution of hot spots looks like? Maxwell equation calculations done in Ref. [10] demonstrate very harp peaks with contrast ≥ 10. Note that the pattern of sharp peaks (hot spots) looks very similar to that in fractal aggregates of nanoscale metallic particles [27].

(2) How low should be the loss in coherent modes? It is known that in strongly pumped laser rods, laser operation supported only by reflections off polished surfaces can occur. The output coupling (loss per round trip) in these cases can be as large as 80-90%. Thus, the coherent modes can be rather "leaky". (However, the estimated above value of the output coupling in the case of a simple closed-loop cavity with isotropic scattering, O.C.>99.999%, appears to be too large to support any coherent mode.)

(3) Why scatterers are so important in the proposed model and why in a non-scattering medium it is not possible to find an ensemble of emitting centers, time delays between which are "just right" to support the coherent state? In non-scattering random medium it is not possible to imagine a high-contract interference pattern determined by point light sources embedded into the medium, unless the distance between light sources is $\geq\lambda$, where λ is the light wavelength. This suggests that in the case of visible light the concentration of emitters should be $<<10^{13}$ cm^{-3}. This value is much smaller than the concentration of excited centers typically used in solid-state random lasers, $>10^{18}$ cm^{-3}. The formation of an interference pattern in

a *scattering* medium is more likely, which is confirmed by numerical calculations [1.10].

In Ref. [1.28], the laser-like emission in a powder of Er doped $LiYF_4$ obtained at cryogenic temperatures was attributed to superfluorescence (in a Dicke-Bonifacio sense [1.29]). Apparently, the self-organization of a coherent state, as shown in Figure 1.2b, has some analogy with the self-organization of cooperative spontaneous emission through coupling with emitted field in the case of superfluorescence. In both cases, the phases of the emitting centers in the ensemble are getting synchronized before the narrow-line, intense, coherent light radiation comes out. However, in the case of superfluorescence, emitting centers adjust (change) their phases of oscillation through interaction via electromagnetic field. In the scheme suggested in this work, nothing changes within emitting centers in the beginning of the process. Just the photon walk paths and the phases of corresponding waves change randomly until a more or less favorable combination realizes. Only when phases are synchronized, interference pattern is formed, and light is partially confined, the emitting centers contributing to the coherent mode start noticing a change, since the density of electromagnetic field in the vicinity of these centers is getting higher. One can say that in the proposed model, in contrast with superfluorescence, synchronization occurs regardless of the phase relaxation time T_2 and, thus, can be expected (and it is observed experimentally) at room temperature.

The difference between the proposed scheme and a simple closed-loop model (inset in Figure 1.1) is that instead of a simple ring cavity, a complex three-

dimensional pattern of multiple reflections and refraction is formed. The superposition of electromagnetic fields leads to the formation of the interference pattern that determines the laser mode. Apparently, scatterers are very efficient in the formation of interference pattern not only when the mean free path l^* is comparable to the light wavelength, but also at much larger values of l^* (10 μm or even 100 μm) when the scattering is reasonably weak. This is in accord with the conclusion above that the coherent emission mode can be rather leaky. Common observation of a speckle pattern in laser light scattered off rough surface with characteristic size of inhomogeneities equal to 100 μm can be used as the evidence of efficient interference pattern formation inside scattering materials with large l^*.

To summarize, a qualitative model explaining appearance of narrow emission peaks in stimulated emission spectra of solid-state random lasers is proposed. The key point of the proposed scheme, which makes it different from simple ASE, is the spontaneous self-organization of the coherent state in a scattering gain medium.

References to Section 1

1.1 V. M. Markushev, V. F. Zolin, Ch.M. Briskina, Sov. J. Quantum Electron., **16**, 281 (1986).

1.2 C. Gouedard *et al.*, JOSA B, **10**, 2358 (1993).

1.3 M. A. Noginov *et al.*, JOSA B, **13**, 2024 (1996).

1.4 H. Cao *et al.*, Appl. Phys. Lett., **73**, 3656 (1998).

1.5 R. M. Laine et al., Materials Science Forum, **343**, 500 (2000).

1.6 R. C. Polson, A. Chipouline, Z. V. Vardeny, Advanced Materials, **13**, 760 (2001).

1.7 H. Cao *et al.*, Appl. Phys. Lett., **75**, 1213 (1999).

1.8 H. Cao *et al.*, Phys. Rev. Lett., **82**, 2278 (1999).

1.9 H. Cao *et al.*, Appl. Phys., Lett., **76**, 2997 (2000).

1.10 H. Cao *et al.*, Phys. Rev. Lett., **84**, 5584 (2000).

1.11 H. Cao, Y. Ling, C. Q. Cao, Phys. Rev. Lett., **86**, 4524 (2001).

1.12 R. C. Polson, J. D. Huang, Z. V. Vardeny, Synthetic Metals, **119**, 7 (2001).

1.13 S. V. Frolov *et al.*, Optics Commun., **162**, 241 (1999).

1.14 N. M. Lawandy *et al.*, Nature **368**, 436 (1994).

1.15 A. A. Lichmanov *et al.*, J of Appl. Spectroscopy, **65**, 818 (1998).

1.16 A. A. Lichmanov *et al.*, "*Experimental studies of the lanthanide doped lasing powders (plasers)*", Proceedings of the International Conference LASERS'98 (Tucson, AZ, Dec. 7-11, 1998), 725 (1999).

1.17 N. È. Ter-Gabriélyan *et al.*, Sov. J. Quantum Electron., **21**, 840 (1991).

1.18 V. F. Zolin, J of Alloys and Compounds, **300-301**, 214 (2000).

1.19 P. C. de Oliveira, J. A. McGreevy, N. M. Lawandy, Opt. Lett., **22**, 700 (1997).

1.20 D. S. Wiersma, A. Lagendijk, Phys. Rev. E, **54**, 4256 (1996).

1.21 S. John, G. Pang, Phys. Rev. A, **54**, 3642 (1996).

1.22 G. A. Berger, M. Kempe, A. Z. Genack, Phys. Rev. E, **56**, 6118 (1997).

1.23 R. M. Balachandran, N. M. Lawandy, J. A. Moon, Opt. Lett., **22**, 319 (1997).

1.24 C. M. Soukoulis, *"Dynamics processes and localization modes in random lasers"*, presented at *OSA Annual Meeting*, October 14-18, 2001, Long Beach, CA; Conference Program, p. 111, paper #ThV1.

1.25 M. A. Noginov *et al.*, Optical Materials., **12**, 127 (1999).

1.26 V. S. Letokhov, Sov. Phys. JETP, **26**, 835 (1968).

1.27 V. M. Shalaev, *"Nonlinear optics of random media: fractal composites and metal/dielectric films"*, Springer Tracts in Modern Physics, Volume 158, Springer-Verlag, Berlin, Heidelberg, 2000, 158 p.

1.28 F. Auzel, P. Goldner, J of Alloys and Compounds, **300-301**, 11 (2000).

1.29 R. Bonifacio, L. A. Lugiato, Phys Rev. A, **11**, 1507 (1975).

1.2 Study of scattering, absorption, and reflection in solid-state random laser

Abstract

Using the coherent backscattering technique, we have measured the transport mean free path lengths l_t for photons in $NdAl_3(BO_3)_4$ powder, a promising solid-state random laser material. The determined value l_t was found to be reasonable at the given average particle size and the index of refraction. Comparing the absorption spectrum of a single crystalline material and the reflection spectrum of powder, we have derived a simple empirical formula for the reflection coefficient of absorbing powder. The proposed formula, which slightly resembles the Lambert-Beer law for transmission, does not correspond to diffusion-dominated migration of photons in a scattering medium.

2.1 Introduction

Determination of the photon mean free path is a substantial fundamental problem in physics of scattering media. It has a special practical significance in the case of solid-state random (powder) lasers [2.1-2.7]. The knowledge of this parameter is important for understanding the regime of operation of random laser [2.8] and for modeling its behavior. The purpose of this work is the quantitative characterization of the scattering process in $NdAl_3(BO_3)_4$ powder, a promising solid-state random laser material. This includes (1) experimental evaluation of the photon transport mean free path l_t, (2) derivation of the relationship between l_t and the mean particle size, and (3) study of the diffused reflection off absorbing powder.

In this work, the transport mean free path l_t (defined as the average distance a wave travels before its direction of propagation is randomized) has been experimentally determined using the coherent backscattering (CBS) technique [2.9-2.11]. Coherent backscattering, a mature experimental method, has proven to give adequate results in suspensions of scatterers in liquids, see for example Refs. [2.12,2.13]. In a number of publications, CBS was used to determine the parameter l_t in solid-state random laser materials [2.14-2.16]. However, the applicability of this method to tightly packed solid-state powders has not been rigorously proven. In the present study, we have theoretically derived the relationship between l_t and the mean particle size s and found that at the given value of the refraction index n, the magnitude of the transport mean free path l_t is quite adequate.

In another particular experiment, we have analyzed the spectrum of diffused reflection $R(\lambda)$ as a function of the effective absorption coefficient $k_{abs}(\lambda)$ of the scattering medium. When we plotted the experimentally obtained diffused reflection coefficient R_{exp} versus the absorption coefficient k_{abs}, we found that the dependence $R_{exp}(k_{abs})$ could be described with a simple empirical formula

$$R_{exp}(\lambda) = exp\left(-\left(xk_{abs}(\lambda)\right)^{1/3}\right), \tag{2.1}$$

slightly resembling the Lambert-Beer formula for absorption, where factor x had units of length.

Our attempt to derive a similar formula, assuming the diffusion character of photon migration in a scattering medium, failed, suggesting that possibly some other mechanisms of photon migration should be considered instead.

2.2 Experimental samples

In our experiments, we used a grounded powder of $NdAl_3(BO_3)_4$ laser crystals grown from flux[1]. The microphotograph of a monolayer of powder has been taken with a scanning electron microscope. Measuring the sizes of particles on the microphotograph, we plotted the histogram $f(d_i)$, portraying the distribution of particles by their sizes, Figure 2.1.

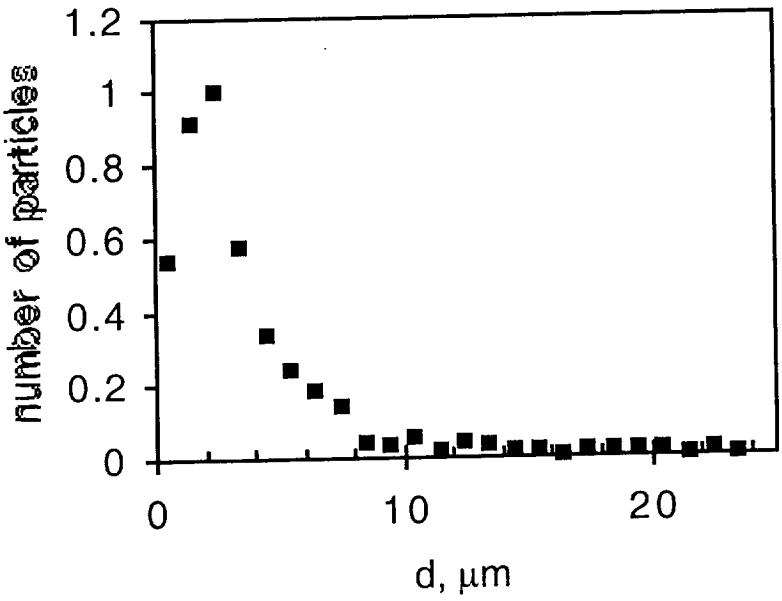

Figure 2.1. Distribution of powder particles by their sizes.

The average particle size, defined as an arithmetic mean, was found to be equal to

$$s = \frac{\sum_i f(d_i)di}{\sum_i f(d_i)}, \qquad (2.1)$$

The porosity of the powder sample placed in 1 mm thick cuvette was equal to 46% (the volume filling factor of crystalline material was equal to 54%).

2.3 Absorption spectra

The absorption spectra of $NdAl_3(BO_3)_4$ single crystal in polarizations *Ellc* and *E_l_c* have been experimentally obtained in Ref. [2.17]. Since the crystal is uniaxial, the "isotropically average" spectrum $\bar{k}_{abs}$ (averaged over *E*||*c* and $E \perp c$ polarizations) can, in the first approximation, be calculated as $\bar{k}_{abs} = (2k_{abs}^{E\perp c} + k_{abs}^{E\|c})/3$, where $k_{abs}^{E\perp c}$ and $k_{abs}^{E\|c}$ are the absorption spectra in polarizations $E \perp c$ and *Ellc*, respectively, Figure 2.2. To calculate the effective absorption spectrum in the porous samples, the absorption spectrum of a single crystal was multiplied by the volume filling factor.

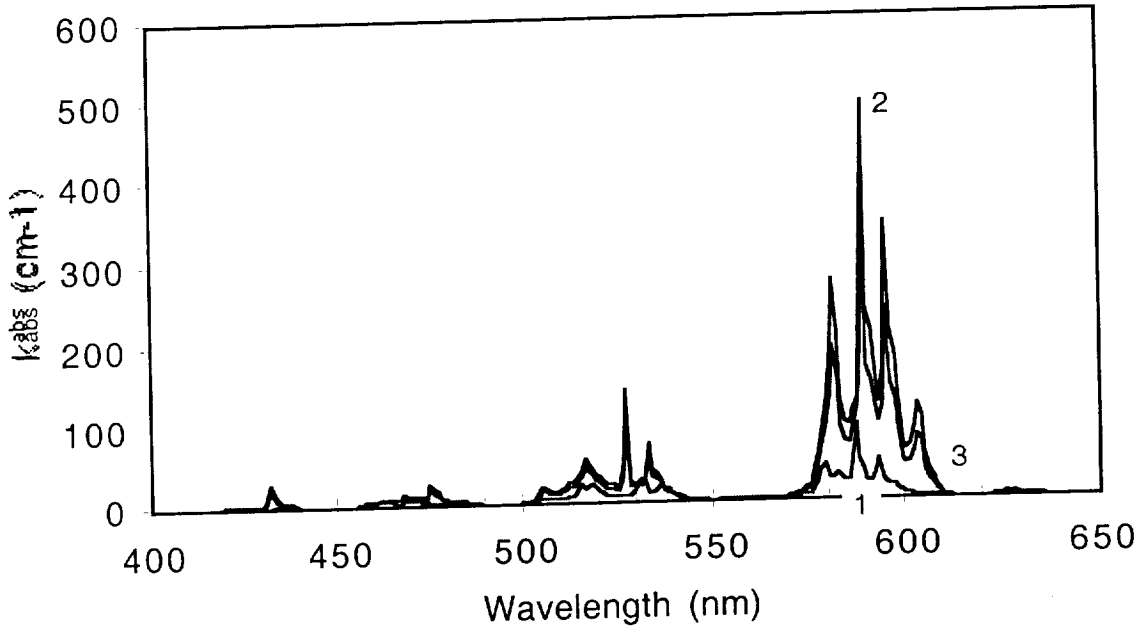

Figure 2.2. Absorption spectrum of $NdAl_3(BO_3)_4$ single crystal; (1) – E_l_c, (2) – Ellc, (3) – averaged spectrum (digitized and recalculated from the transmission spectra published in Ref. [2.9]).

[1] The crystals were grown in the lab. of Prof. G. Huber, Hamburg University, Germany

2.4 Coherent backscattering experiment

2.4.1 Idea of coherent backscattering

Coherent backscattering (CBS) has been first experimentally demonstrated in pioneering works [2.9-2.11] where enhanced scattering intensities ("cones") have been observed in the exact backscattering direction. Photons incident onto scattering medium experience smaller or larger number of (random) scattering events until they leave the medium through the front surface or are getting absorbed. However, light is a wave and the light diffusion process should be described by amplitudes rather than by probabilities [2.18]. Any random path of light inside a scattering medium can be "time reversed" and followed in the opposite direction. Two photons counterpropagating along the same optical path have equivalent phase delays. Thus, if two partial waves entering the same optical path from the opposite ends are in phase, they will be also in phase when they leave the sample, causing constructive light interference in the exact backscattering direction. The theoretical model describing the shape of the CBS cones in diffusion approximation [2.13,2.19,2.20] allows one to determine the parameters l_t and k_{abs} by fitting the experimental curve with the calculated one.

2.4.2 Experimental setup

In the measurements of the CBS cones, we used a standard setup depicted in Figure 2.3. A low divergence (< 0.45 mrad) Spectra-Physics Beamlok Argon-ion laser was used as a light source. The linearly polarized laser beam ($1/e^2$ waist =1.7 mm) was sent to the sample via a beam splitter. The light power incident onto the sample did

not exceed 10 mW. The direct beam transmitted through the beam splitter was carefully dumped. The CBS cones were recorded at four different wavelengths of Ar laser, 457.9 nm, 488 nm, 496.5 nm, and 514.5 nm.

The angular distribution of the backscattered light intensity was recorded using a photodiode mounted on a motorized translation stage, Figure 2.3. The distance between a silicon photo-detector and the sample was equal to ≈87.5 cm. A mask with small pinhole (0.5 mm diameter) was placed in front of the detector. The corresponding angular resolution in our experiment, predominantly determined by the finite size of the laser spot on the sample, was approximately equal to 2 mrad. The scanning rate was set to ≈0.027 mrad/s. The detection was performed in the polarization-conserving channel.

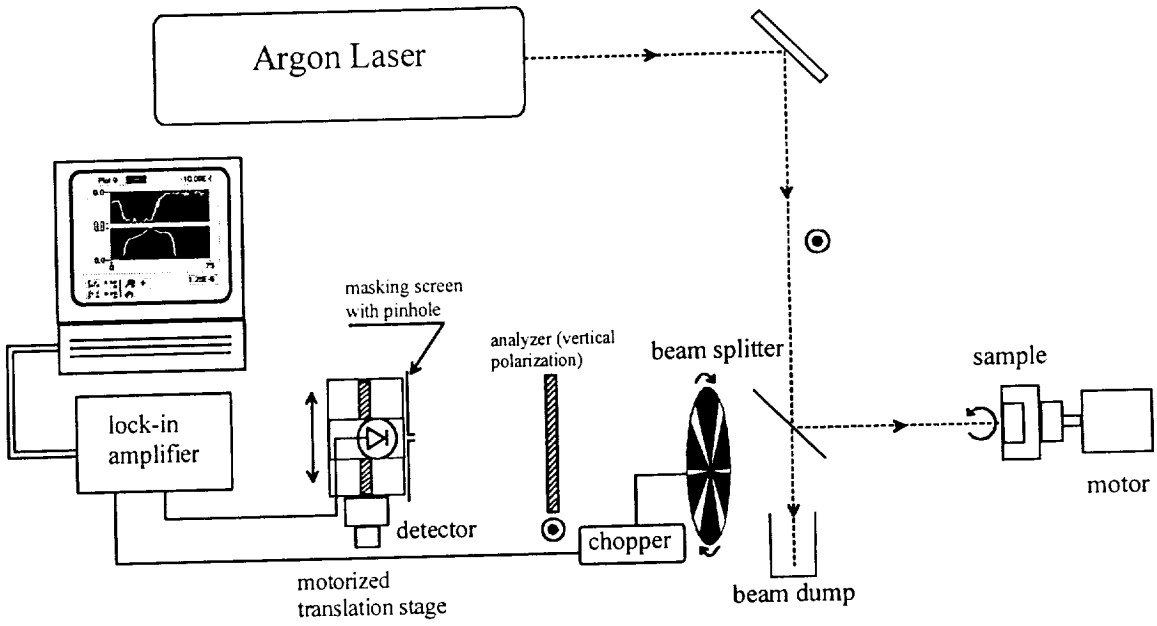

Figure 2.3. Setup for the coherent backscattering measurements.

The plane of the cuvette wall was slightly tilted from the normal to the incident beam in order to prevent the specular reflection from reaching the detector. The sample was mounted on a motorized spinning holder to provide for the averaging over speckle patterns, Figure 3. The best attempt was made to eliminate stray light scattered off various surfaces and optical components.

The chopping of the backscattering light and the use of the lock-in amplifier helped us to suppress the contribution of residual parasitic lights (reflection, scattering, etc.) to the recorded signal. The signal from the lock-in amplifier was transferred to a computer via GPIB interface.

2.4.3 Experimental results

As an example, the CBS cone obtained at 488 nm is shown in Figure 2.4. The solid line in Figure 2.4 is the theoretical fit to the experiment.

The theoretical curve, as given in Refs. [2.13,2.19,2.20], was fitted to the experimental data with the following adjustable coefficients: (1) the transport mean free path l_t; (2) the enhancement factor; (3) a numerical factor that scales the y-axis, whereas the absorption coefficient is taken fixed as from the absorption data. The transport mean free path determines the width of the backscattering cone, whereas the ratio between top and diffuse background is determined by the enhancement factor. The enhancements factors for the cones recorded at different wavelengths, defined as the ratio between the intensity scattered in the exact backward direction and the diffuse background, range between 1.6 and 1.8. These numbers (common for vertical polarization measurements in which single scattering cannot be

eliminated) are smaller than the maximum theoretically possible value equal to 2. The results of the fitting are summarized in Table 2.1.

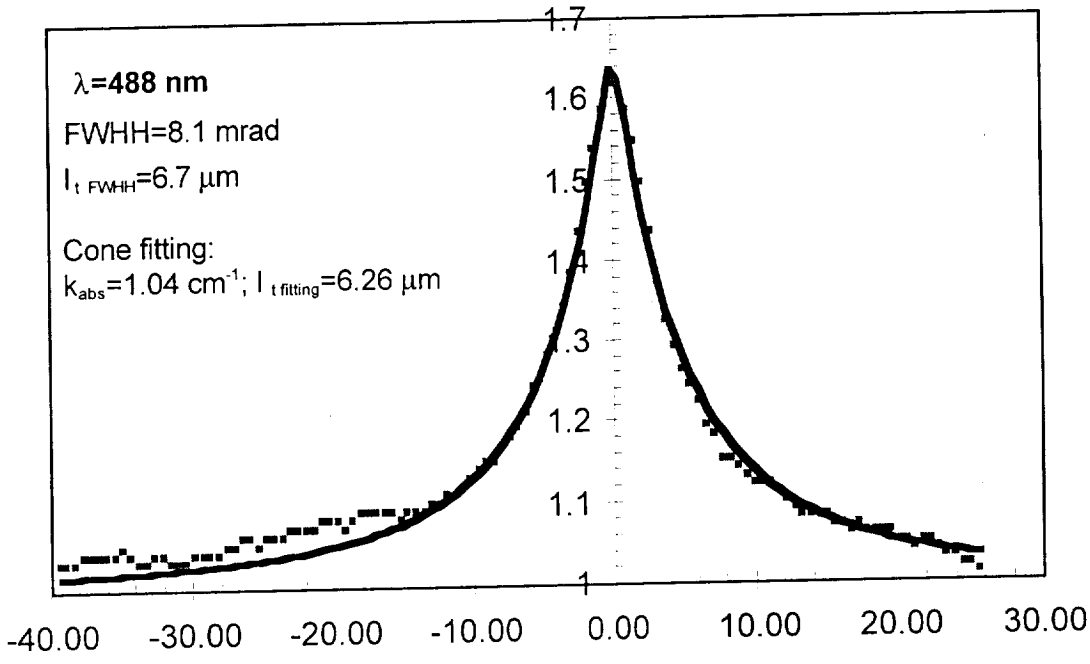

Figure 2.4. CBS cone in $NdAl_3(BO_3)_4$ powder at 488 nm. Squares – experiment, solid line – diffusion theory.

Table 2.1

Wavelength, nm	k_{abs}, cm^{-1}	FWHM, mrad	l_t, μm (cone fitting)	l_t, μm (FWHM)
514.5	15.4	9.3	7.64	6.2
496.5	0.46	8	6.32	6.9
488	1.04	8.1	6.26	6.7
457.9	3.21	8.3	6.74	6.1

The average value of l_t calculated with this method is equal to $l_{t\ cone\ fitting}$=6.7 μm (the point at λ=476 nm is not included in the average). Thus, in $NdAl_3(BO_3)_4$ powder at the laser wavelengths used, the maximum product $(k_{abs}l_t)_{max}$ is approximately equal to 10^{-2}. We hypothesize that at $(k_{abs}l_t)_{max}<<1$, the absorption in the medium can be neglected and the transport mean free path l_t can be calculated from the full width at half maximum (FWHM) W of the CBS cones [2.13,2.19,2.20],

$$l_t \approx 0.7\frac{\lambda}{2\pi W}, \tag{2.3}$$

where λ is the light wavelength. Obviously, this second method is much easier to use than the first one. The average value of the transport mean free path determined from FWHM is equal to $\bar{l}_{t\ (FWHM)}$=6.5 μm, very close to $l_{t\ (cone\ fitting)}$ determined by the first method.

2.4.4 Correlation between transport mean free path l_t and free particle size s

The concepts of the scattering mean free path l_s and the transport mean free path l_t have been originally introduced in the literature to describe scattering in media where the average distance between particles is significantly larger than the particle size. This is not the case of tightly packed powders.

In the first approximation, tightly packed powder (with large filling factor) can be modeled as an almost monolithic solid with air gaps crossing it in all directions. We assume that the air gaps are not exactly plane-parallel, although they are not very far from being plane-parallel, Figure 5a.

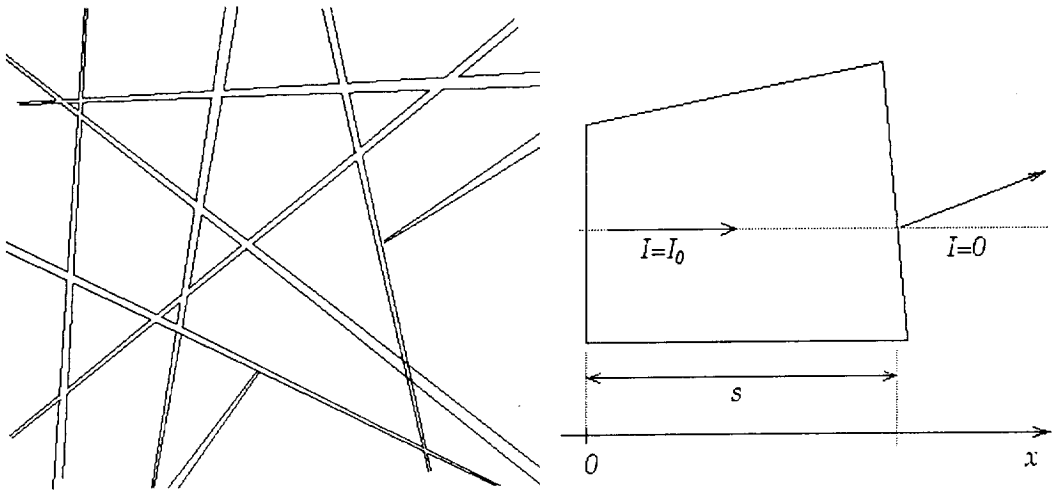

(a) (b)

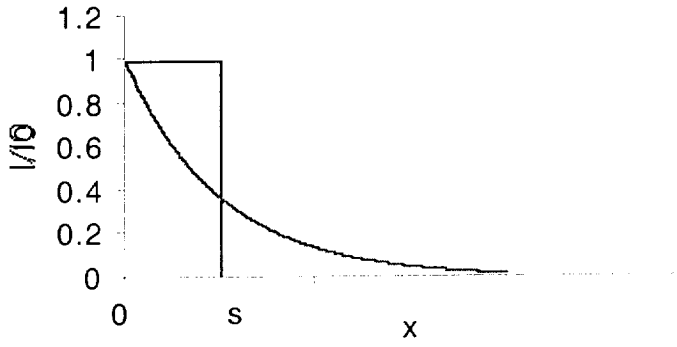

(c)

Figure 5. (a) Schematic drawing of tightly packed powder, (b) propagation of a photon flux inside a particle, (c) step-like distribution of the photon flux intensity I(x) and approximating it exponential function.

By definition, the scattering mean free path l_s is the length at which the intensity of photon flux (plane-wave) fallen onto the sample is reduced by a factor $1/e$. This definition assumes that (1) all photons, which directions of propagation have been disturbed, even slightly, are lost for the original photon flux, (2) the decay of the

original photon flux is exponential, $\propto e^{-l_s x}$, and (3) all surface effects at the boundary between the sample and air are neglected.

The flux of photons propagating along the direction $\vec{x}$ inside a particle is not disturbed until the flux reaches the particle wall at $x=s$ ($I(x)=I_0$ at $x \leq s$) and it is totally refracted at $x=s$ (correspondingly, at $x>s$ the intensity of the original flux propagating in the direction $\vec{x}$ is equal to zero), Figure 5b. The plot of the function $I(x)$ (a step function) is shown in Figure 5c. The most adequate fit of the step-function $I(x)$ with the exponential function $I_0 e^{-l_s x}$ is such that conserves the area under the $I(x)$ trace,

$$\int_0^\infty I_0 e^{-l_s x} dx = \int_0^\infty I(x) dx = \int_0^s I_0 dx, \tag{2.4}$$

yielding $l_s=s$. Thus, in the first approximation, in tightly packed powder, the scattering mean free path l_s can be assumed to be equal to the average particle size s.

The transport mean free path l_t, can be calculated from l_s using the formula

$$l_t = \frac{1}{1-\langle cos(\theta) \rangle} l_s, \tag{2.5}$$

where $\langle \cos(\theta) \rangle$ is the average cosine of the scattering angle for each scattering event.

We calculated $\langle \cos(\theta) \rangle$ assuming that scatterers are (plane-parallel) air gaps separating different particles in a powder. In our model, when the angle of incidence was smaller than the angle of total internal reflection φ_{crit}, the reflection

coefficients of the material-air boundaries were calculated according to the Raleigh formula

$$\rho_{\perp} = \left(\frac{n_1 \cos(\varphi) - n_2 \cos(\psi)}{n_1 \cos(\varphi) + n_2 \cos(\psi)} \right)^2 \quad \text{and} \tag{2.6a}$$

$$\rho_{\parallel} = \left(\frac{n_2 \cos(\varphi) - n_1 \cos(\psi)}{n_2 \cos(\varphi) + n_1 \cos(\psi)} \right)^2, \tag{2.6b}$$

where $\rho_{\perp}$ was the reflection coefficient for light polarized in the direction perpendicular to the plane of incidence, $\rho_{\parallel}$ was the reflection coefficient for light polarized in the plane of incidence, n_1 was the refraction index of the crystalline material, n_2=1 was the refraction index of air, φ was the angle of incidence in the crystalline medium (we assumed the scenario depicted in Figure 2.5b), and ψ was the propagation angle of the refracted light inside of the air gap. The corresponding angles and light rays are shown in Figure 2.6.

We assumed that light was arbitrary polarized. Thus, in our calculations, we have used some effective reflection coefficient ρ calculated as

$$\rho = \sqrt{\frac{\rho_{\perp}^2 + \rho_{\parallel}^2}{2}}. \tag{2.7}$$

To take into account the effect of two material-air boundaries associated with every band gap, we used the effective reflection and transmission coefficients calculated as

$$\rho_{eff} = 2\rho - \rho^2 \text{ and} \tag{2.8a}$$

$$\tau_{eff} = 1 - 2\rho + \rho^2. \tag{2.8b}$$

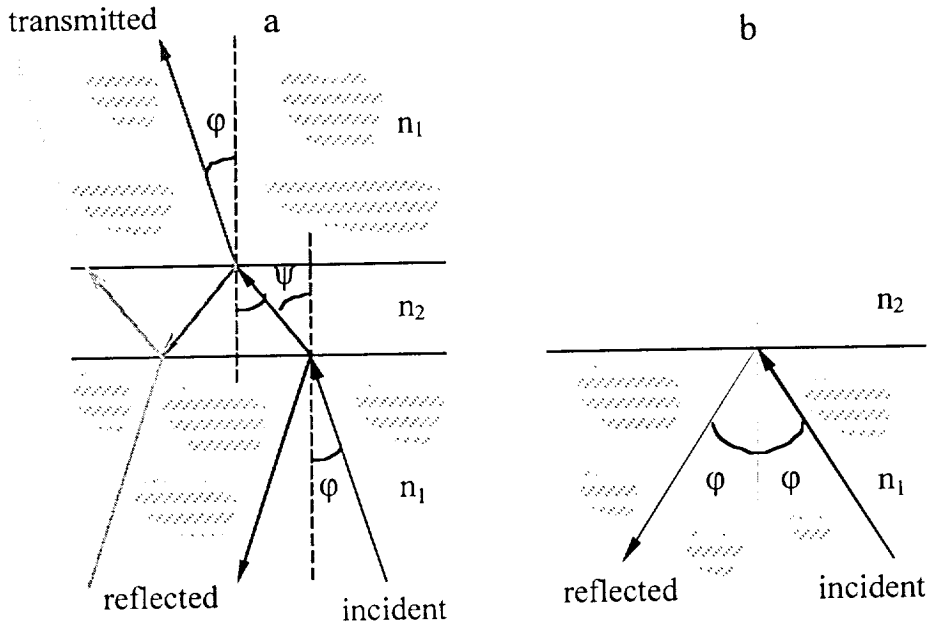

Figure 2.6. (a) Refraction of a light beam at the crystalline-air boundaries separating two particles of powder, (b) total internal reflection scenario.

The critical angle φ_{crit} was calculated according to the Snell's law

$$\sin(\varphi_{crit})n_1 = \sin(\pi/2)n_2. \tag{2.9}$$

At the incidence angles larger than φ_{crit}, scattering event manifests itself as total internal reflection. In order to calculate the average cosine of the scattering angle $\langle\cos(\theta)\rangle$, we took an integral over incidence angles φ ($0<\varphi<\pi/2$), at each angle accounting for the intensities and the directions of the reflected and transmitted beams (the integral was normalized by 2π). The calculated dependence of $\frac{l_t}{l_s} = \frac{1}{1-\langle\cos(\theta)\rangle}$ on the index of refraction n_1 is shown in Figure 2.7.

As follows from Figure 2.7, in a wide range of the practically important values of n_1 ($1.6<n_1<3.2$), the ratio l_t/l_s is nearly constant, $l_t/l_s=2.0\pm0.4$.

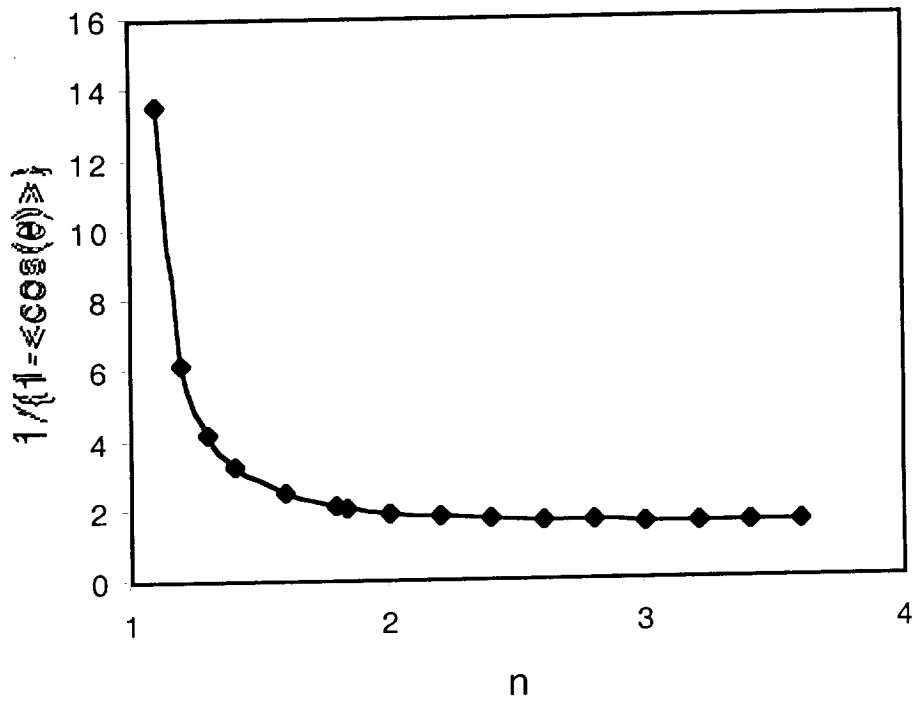

Figure 2.7. Calculated dependence $\frac{1}{1-\langle cos(\theta)\rangle}$ *versus* n_1.

As follows from Figure 2.7, in a wide range of the practically important values of n ($1.6<n<3.2$), the ratio l_t/l_s is almost constant, $l_t/l_s=2.0\pm0.4$.

We assumed that the index of refraction in $NdAl_3(BO_3)_4$ was equal to ≈1.84, close to that in a relevant laser crystal $LaSc_3(BO_3)_4$ [2.21]. At this value of n_1, $\frac{l_t}{l_s}=\frac{1}{1-\langle cos(\theta)\rangle}$=2.07. If l_s is equal to the average particle size s=3.55 μm, than the calculated transport mean free path would be equal to 7.3 μm, which is reasonably close (within 10%) to the value l_t=6.7 μm obtained from the CBS cone fitting.

Thus, the value of the transport mean path length l_t obtained in the CBS experiment appears to be reasonable at the given index of refraction and particle

size distribution. This also validates the proposed model that allows one to determine l_t in tightly packed powders if the particle sizes and the index of refraction are known.

Note that Rayleigh formulas 6a and 6b are valid only when the particle size is large, ideally $s>>\lambda$. As we demonstrate in this work, adequate results can be obtained at $s/\lambda\approx7$. Surprisingly, the model can predict the correct order of magnitude of l_t even in the case of nanoparticles ($s<\lambda$). Thus, in ZnO nanopowders, the ratios l_t/s were equal to ≈3.2 (s=100 nm) [2.22] and ≈4 (s=50 nm) [2.23]. The index of refraction in ZnO is equal to 2.008 and 2.029 for two different crystallographic directions [2.24]. Thus, according to our simple model (Figure 2.7), the ratio l_t/s in ZnO powder with large particle sizes should be equal to 1.9, which is still not so far from the experimental values obtained in nanopowders, 3.2 and 4.

2.5 Reflection spectra measurements and results

The reflection spectrum of $NdAl_3(BO_3)_4$ powder was taken using LAMBDA 20 spectrophotometer from Perkin Elmer. A special integrating sphere assembly allowed one to collect diffused light reflected into the spherical angle 2π. The transmission of the samples was much less than 1%. Thus, we considered our samples to be infinitely thick.

The cuvette with $NdAl_3(BO_3)_4$ powder was set normal to the incident light beam. In this configuration, light reflected off the glass wall of the cuvette left the integrating sphere through the opening for the incident beam and, thus, did not contribute to the diffused reflection signal.

The appropriate normalizations of the recorded spectra to the reflection of the diffused ideally white standard reference sample and other tilted and normally oriented diffused white reflectors have been made. These normalizations corrected for the spectral response of the apparatus, loss of light through the entrance port of the integrating sphere, and the loss caused by the tiny black paper screen masking the edges of the cuvette. The resulting reflection spectrum is shown in Figure 2.8.

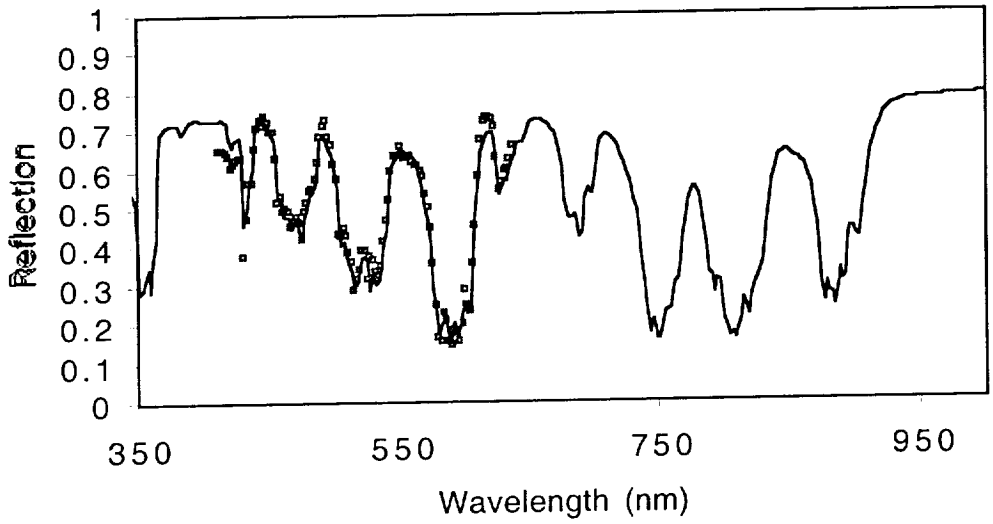

Figure 2.8. Reflection spectrum of $NdAl_3(BO_3)_4$ powder. Experiment – solid line, calculation (according to Eq. (2.1) with k_{abs0}=0.3 cm^{-1} and x=0.08 cm) – squares.

The spectrum in Figure 2.8 is the result of the *absolute* measurements. No "forced" adjustments of the100% base line have been made. As follows from Figure 2.8, the experimentally determined reflection coefficient is not equal to 1 at λ>980 nm, the spectral region where trivalent Nd ions do not have absorption [2.25]. The experiment has been done with high accuracy and the 17% discrepancy (the difference between 100% ideal reflection and experimentally obtained 83%

reflection at >980 nm) is too much for the experimental error. The deviation of the reflection coefficient at 1 μm from unity can be explained by (1) contamination of powder and ceramic by, presumably spectrally gray, material of the mortar and pestle which were used to pulverize $NdAl_3(BO_3)_4$ crystals or (2) surface absorption of the microcrystallines. When a piece of white paper was placed in the experimental setup instead of the powder sample, the measured refection coefficient was as high as 97%-98%. Note that if some small experimental error took place, it influenced primarily the regions of the reflection spectrum corresponding to weak absorption and practically did not affect the spectral regions of strong absorption.

A spectrum of diffused reflection $R(\lambda)$, in zero approximation, resembles a regular transmission spectrum of non-scattering sample $T(\lambda)$. In both cases, the intensity of light coming out of the sample is reduced because of filtering that occurs when light travels over the distance d in a medium with absorption. In the case of a transmission spectrum (in non-scattering medium), the distance d is simply the thickness of the sample.

If the transmission T and the absorption coefficient k_{abs} are known, the length of the light path inside the sample, d, can be determined from a known Lambert-Beer formula

$$T(\lambda) = \frac{I_{out}(\lambda)}{I_{in}(\lambda)} = \exp\left(-k_{abs}(\lambda)d\right), \tag{2.10}$$

where I_{out} and I_{in} are the intensities of incident and transmitted light, respectively. Here, the reflection of light by the surfaces of the sample is neglected for simplicity, if necessary it can be easily taken into account.

In a scattering sample, different photons travel over different paths, until they come out through the front surface or are getting absorbed in the medium (we assume that a sample is infinitely thick and neglect transmission). Obviously, the effective average path-length, which photons travel within the sample, should reduce with the increase of the absorption coefficient. Because of an apparent similarity between reflection and transmission spectra, we decided to apply a formula similar to Eq. (2.10) to the reflection spectrum $R(\lambda)$ in order to obtain the effective average path-length $d(k_{abs}(\lambda))$,

$$d\left(k_{abs}(\lambda)\right) = -\frac{\ln\left(R(\lambda)\right)}{k_{abs}(\lambda)}. \qquad (2.11)$$

(Evidently, the value $d(k_{abs}(\lambda))$ is not equal to the arithmetic average of all path-lengths of photons that leave the sample.)

The dependence $d(k_{abs}(\lambda))$ in $NdAl_3(BO_3)_4$ powder is plotted in log-log scale in Figure 2.9 (circles). One can see that at high values of the absorption coefficient, this dependence can be approximated with a straight line having a slope equal to -2/3. As we have discussed above, some (presumably gray) parasitic absorption k_{abs0} may be present in our powder. The effective absorption of a scattering sample k^*_{abs} is a sum of this parasitic absorption and k_{abs},

$$k^*_{abs}(\lambda) = k_{abs}(\lambda) + k_{abs0}, \qquad (12)$$

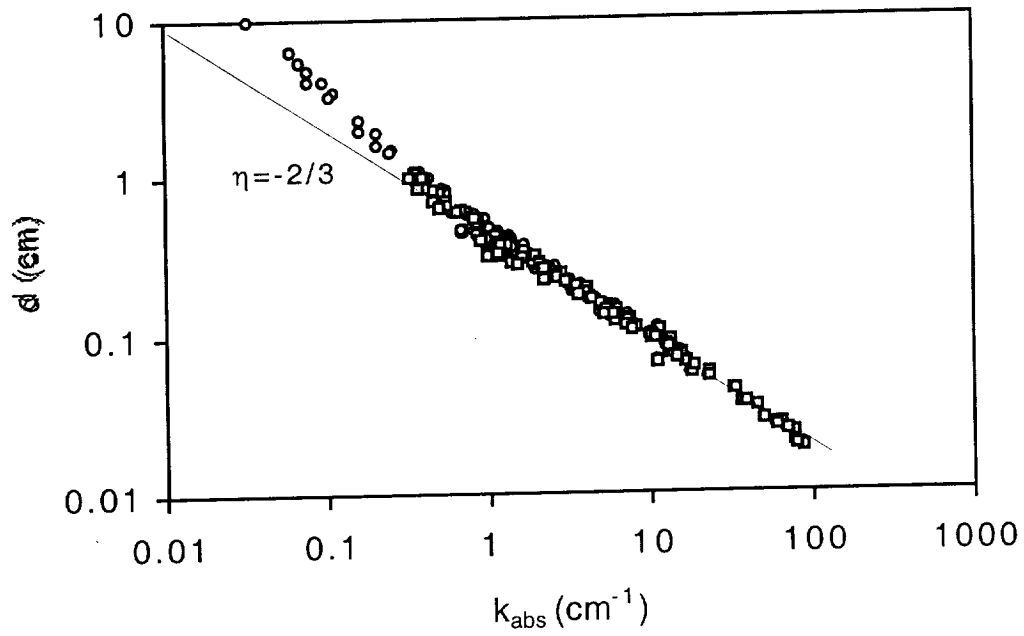

Figure 2.9. The dependence d *vs.* $k_{abs}(\lambda)$ in $NdAl_3(BO_3)_4$ powder. Circles – k_{abs0}=0, squares – k_{abs0}=0.3 cm^{-1}.

By choosing an appropriate value of k_{abs0}, 0.3 cm^{-1}, one can make the dependence in Figure 2.9 linear in the whole range of the absorption coefficients (squares). In the range of large absorption coefficients, >1 cm^{-1}, the two traces in Figure 2.9 overlap. The adjustment of the absorption coefficient above seems to be reasonable. However, there is no direct independent measurement that can confirm this number.

Thus, we conclude that the dependence

$$d = \left(\frac{x}{\left(k^{*}_{abs}(\lambda)\right)^2} \right)^{1/3} \qquad (2.13)$$

takes place at k_{abs}^{*}>1 cm^{-1} and possibly at smaller values of k_{abs}^{*}.

Combining Equations (2.11) and (2.13), one obtains the empirical Formula (2.1) for the diffused reflection coefficient of a scattering powder or ceramic. This formula is almost as simple as the Lambert-Beer's formula for transmission. As follows from Figure 2.8, at the appropriate choice of the parameter x Formula (2,1) reconstructs the experimental spectrum R(λ) with pretty high accuracy.

2.6 Discussion of reflection

In diffusion approximation, the formula for diffused reflection coefficient $R(k_{abs})$ can be derived as follows. Let F [$cm^{-2}s^{-1}$] be the flux of photons incident onto the surface of semi-infinite scattering medium. The distribution of photon density $u(x)$ [cm^{-3}] inside the medium is given by equation

$$\frac{\partial u}{\partial t} = D\frac{\partial^2 u}{\partial x^2} - \frac{c}{n}k_{abs}u, \tag{2.14}$$

where D is the diffusion coefficient, x is the distance in the direction normal to the surface of the sample (x=0 at the sample surface), c is the speed of light, n is the refraction index, and k_{abs} is the average absorption coefficient of the medium.

The steady-state solution of Eq. (2.14) reads

$$u(x) = u(0)e^{-x/\delta}, \tag{2.15}$$

where u(0) is the photon density inside the medium at $x \to +0$ and $\delta = \sqrt{\frac{Dn}{k_{abs}c}}$ is the effective penetration depth. The density of photons in the incident flux (outside the sample) is given by

$$u_i = \frac{F}{c}. \tag{2.16}$$

One can argue that

$$u(0)=\zeta u_i n, \tag{2.17}$$

where ζ is the multiplication factor greater than 1. In this case, the total rate of photon absorption inside the medium (per unit area) is given by

$$K=\int_0^\infty k_{abs}\zeta F e^{-\frac{x}{\delta}}dx=\zeta F\sqrt{\delta k_{abs}}=\zeta F\sqrt{\frac{n}{c}k_{abs}D}\quad [\text{in cm}^{-2}\text{s}^{-1}]. \tag{2.18}$$

Accordingly, the reflection coefficient in the diffusion approximation can be calculated as

$$R_{diff}^{calc}=1-\frac{K}{F}=1-\zeta\left(\frac{nD}{c}k_{abs}\right)^{\frac{1}{2}}. \tag{2.19}$$

In scattering medium without absorption

$$D=\frac{cl_t}{3n}; \tag{2.20}$$

thus, in the first approximation,

$$R_{diff}^{calc}=1-\frac{\zeta}{\sqrt{3}}\left(l_t k_{abs}\right)^{\frac{1}{2}}. \tag{2.21}$$

On the other hand, at $(xk_{abs})^{1/3}<<1$, the empirical formula for the reflection coefficient (1) can be rewritten as

$$R_{exp}=1-\left(xk_{abs}\right)^{\frac{1}{3}}=1-\xi\left(l_t k_{abs}\right)^{\frac{1}{3}}. \tag{2.22}$$

(Here we expressed x in terms transport mean free path l_t and factor ξ, $x=\xi^3 l_t$).

Equations (2.21) and (2.22) have an apparently similar form but the different power dependence on k_{abs}. In Figure 2.10, the experimental and the calculated (according to Eq. (2.21)) reflection coefficients are plotted as $ln(-ln(R))$ vs $ln(k_{abs})$. One can see that the experimental dependence has characteristic slope equal to $\eta=1/3$ while the

theoretical one has a different slope equal to $\eta=1/2$. At large values of k_{abs}, the calculated curve deviates from the straight line since the term $\frac{\zeta}{\sqrt{3}}(l_t k_{abs})^{\frac{1}{2}}$ is getting large and more terms would be needed in the Taylor series is order to adequately describe an exponent.) This suggests that the character of photon migration in the studied powder is different from diffusion. Note that a possible deviation from the diffusion regime of migration in $Nd_{0.5}La_{0.5}Al_3(BO_3)_4$ ceramic random laser has been reported in Ref. [2.26].

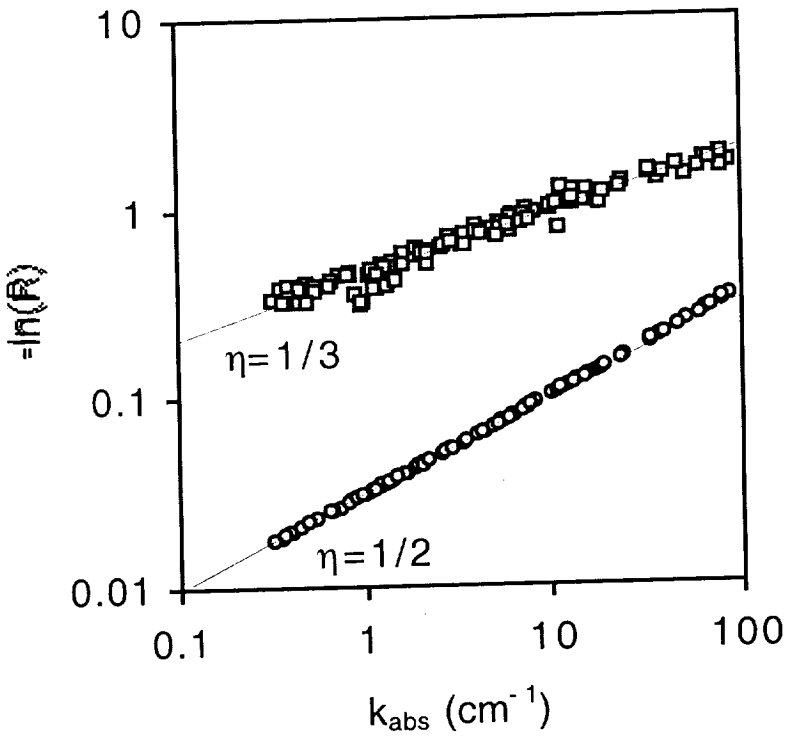

Figure 2.10. -ln(R) plotted vs. k_{abs}. Squares – experiment, circles – calculation according to the formula derived in the assumption of photon diffusion.

According to Ref. [2.27] (which draws an analogy with a nuclear fusion process), in the scattering medium with absorption, the diffusion coefficient depends on the absorption in the medium,

$$D = \frac{\Sigma_s}{3\Sigma(\Sigma - \overline{\mu}\Sigma_s)}, \tag{2.23}$$

where $\Sigma_s=1/\Lambda_s$ (Λ_s is the scattering mean free path), $\Sigma_a=1/\Lambda_a$ (Λ_a is the absorption length), $\Sigma=\Sigma_s+\Sigma_a$, and $\overline{\mu}$ is the average cosine of the scattering angle. Substituting Eq. (2.23) to Eq. (2.19), one obtains a more complicated dependence of the reflection coefficient on k_{abs} than that given by Eq. (2.21). However, the most important power term in the series is still $\propto k_{abs}^{1/2}$ and the slope of the dependence $ln(-ln(R))$ vs $ln(k_{abs})$ is still equal to 1/2 but not to 1/3.

The simple model above assumes a sharp (step-like) increase of the photon density at the surface of the sample. More accurate calculations, based on the balance of photon fluxes in the vicinity of the surface ($x\rightarrow+0$) lead to expressions more complicated than Eq (2.21). However, the dominant power term in the equation is still $\propto k_{abs}^{1/2}$ and the slope of the dependence $\ln(-\ln(R))$ vs $\ln(k_{abs})$ is still close to 1/2.

2.7 Summary

We have studied coherent backscattering (CBS) and diffused reflection in a powder of $NdAl_3(BO_3)_4$, a promising solid-state random laser material. The shapes of the CBS cones have been analyzed to determine the value of the transport mean free path l_t. It was shown that at the given mean particle size s=3.5 μm and maximum

absorption coefficient k_{abs}<500 cm^{-1}, l_t can be obtained with high accuracy from simple measurements of the width of the CBS cone. The model, which allows to calculate l_t in tightly packed powder if the mean particle size and the index of refraction are known, has been developed. A good agreement between the experiment and the model has been demonstrated.

Comparing the diffused reflection spectrum of $NdAl_3(BO_3)_4$ powder with the absorption spectrum collected in a single crystal of the same material, we have obtained a simple empirical formula for the diffused reflection coefficient R. The structure of the formula slightly resembles that of the Lambert-Beer formula for transmission. The calculations suggest that photon migration in tightly packed ceramic is not a diffusion and that the diffusion character of motion in scattering media should not always be assumed *a priori*.

References to Section 2

2.1 V. M. Markushev, V. F. Zolin, Ch. M. Briskina, "Luminescence and stimulated emission of neodymium in sodium lanthanum molybdate powders", Sov. J. Quantum Electronics, **16**, pp. 281-283 (1986).

2.2 C. Gouedard, D. Husson, C. Sauteret, F. Auzel, A. Migus, "Generation of Spatially incoherent short pulses in laser-pumped neodymium stoichiometic crystals and powders", J. Opt. Soc. Am. B, **10**, pp. 2358-2363 (1993).

2.3 M. A. Noginov, N. E. Noginova, H. J. Caulfield, P. Venkateswarlu, T. Thompson, M. Mahdi, V. Ostroumov, "Short-pulsed stimulated emission in the powders of $NdAl_3(BO_3)_4$, $NdSc_3(BO_3)_4$, and Nd:$Sr_5(PO_4)_3F$ laser crystals", J. Opt. Soc. Am. B, **13**, pp. 2024-2033 (1996).

2.4 H. Cao, Y. G. Zhao, H. C. Ong, S. T. Ho, J. Y. Dai, J. Y. Wu, R. P. H. Chang, "Ultraviolet lasing in resonators formed by scattering in semiconductor polycrystalline films", Appl. Phys. Lett., **73**, pp. 3656-3658 (1998).

2.5 R. M. Laine, T. Hinklin, G. Williams, S. C. Rand, "Low-cost nanopowders for phosphor and laser applications by flame spray pyrolysis", Materials Science Forum, **343**, pp. 500-510 (2000).

2.6 R. C. Polson, A. Chipouline, Z. V. Vardeny, "Random lasing in p-conjugated films and infiltrated opals", Advanced Materials, **13**, pp. 760-764 (2001).

2.7 M. A. Noginov, N. Noginova, S. U. Egarievwe, H. J. Caulfield, C. Cochrane, J. C. Wang, M. R. Kokta, J. Paitz, "Study of the pumping regimes in Ti-sapphire and $Nd_{0.5}La_{0.5}Al_3(BO_3)_4$ powders", Optical Materials, **10**, pp. 297-303 (1998).

2.8 D. S. Wiersma, A. Lagendijk, "Light diffusion with gain and random lasers", Phys. Rev. E, **54**, pp. 4256-4265 (1996).

2.9 Y. Kuga and A. Ishimaru, "Retroreflectance from a dense distribution of spherical particles," J. Opt. Soc. Am. A, **1**, pp. 831-836 (1984).

2.10 M. P. van Albada, and A. Lagendijk, "Observation of weak localization of light in random medium," Phys. Rev. Lett., **55**, pp. 2693-2695, (1985).

2.11 P. E. Wolf and G. Maret, "Weak localization and coherent backscattering of photons in disordered media," Phys. Rev. Lett., **55**, pp. 2696-2699 (1985).

2.12 P. E. Wolf, G. Maret, E. Akkermans, and R. Maynard, "Optical coherent backscattering by random media: an experimental study," J. Phys. France, **49**, pp. 63-75 (1988).

2.13 M. B. van der Mark, M. P. van Albada, and A. Lagendijk, "Light scattering in strongly scattering media: Multiple scattering and weak localization," Phys. Rev. B, **37**, pp. 3575-3592 (1988).

2.14 H. Cao, J. Y. Xu, D. Z. Zhang, S. H-. Chang, S. T. Ho, E. W. Seelig, X. Liu, and R. P. H. Chang, "Spatial confinement of laser light in active random media," Phys. Rev. Lett., 84, pp. 5584-5587 (2000).

2.15 S. C. Rand, "Strong localization of light and photonic atoms," Can. J. Phys., **78**, pp. 625-637 (2000).

2.16 R. C. Polson, J. D. Huang, and Z. V. Vardeny, "Random lasers in π-conjugated polymer films," Synthetic Metals, **119**, pp. 7-12 (2001).

2.17 H.-D. Hattendorf, Dissertation zur Erlangung des Doktorgrades des Fachbereich Physik (Universität Hamburg, Hamburg, Germany, 1994).

2.18 S. John, "Localization of light", Physics Today, pp. 32-40, May 1991.

2.19 E. Akkermans, P.E. Wolf, and R. Maynard, "Coherent backscattering of light by disordered media: Analysis of the peak line shape," Phys. Rev. Lett., **56**, 14, pp. 1471-1474 (1986).

2.20 E. Akkermans, P.E. Wolf, R. Maynard, and G. Maret, "Theoretical study of the coherent backscattering of light by disordered media," J. Phys. France, **49**, pp. 77-98 (1988).

2.21 S. T. Durmanov, O. V. Kuzmin, G. M. Kuzmicheva, S. A. Kutovoi, A. A Matrynov, E. K. Nesynov, V. L. Panyutin, Yu. P. Rudnitsky, G. V. Smirnov, V. L. Hait, V. I. Chizhikov, "Binary rare-earth scandium borates for diode-pumped lasers", Opt. Mater., **18**, pp. 243-284 (2001).

2.22 H. Cao, Y. G. Zhao, S. T. Ho, E. W. Seelig, Q. H. Wang, and R. P. H. Chang, "Random Laser Action in Semiconductor Powder," Phys. Rev. Lett., **82**, pp. 2278-2281 (1999).

2.23 H. Cao, J.Y. Xu, D. Z. Zhang, S.-H. Chang S. T. Ho, E.W. Seelig, X. Liu, and R. P. H. Chang, "Spatial Confinement of Laser Light in Active Random Media," Phys. Rev. Lett., **84**, 5584-5587 (2000).

2.24 V. A. Rabinivich, Z. Ya. Khavin, "Short handbook on chemistry" ("Kratkii khimicheskii spravochnik"), Khimia, Leningrad (1977) 376 p. (in Russian)

2.25 A. A. Kaminskii, "Crystalline lasers: Physical processes and operation schemes", CRC Press, Boca Raton, New York, London, Tokyo, pp. 561 (1996).

2.26 M. A. Noginov, M. Bahoura, K. Morris, N. Noginova, "Random laser without diffusion?", will be presented at QELS-2002 conference.

2.27 V. S. Letokhov, "Generation of light by a scattering medium with negative resonance absorption", Sov. Phys. JETP, **26**, pp. 835-840 (1968).

1.3 Summary of results obtained during 2nd year (2001-02) of NCC-1-01049 NASA project by the Purdue University group in cooperation with the NMSU group

1. It is shown that in metal-dielectric percolation films, sub-wavelength localization of plasmon modes in the space domain may result in sub-cycle field fluctuations in the time domain. The modes in such semicontinuous metal films are localized in nm-sized areas, "hot-spots," where EM-field is extremely enhanced. When the excitation pulse has a broad spectrum, sub-femptosecond optical responses can occur locally on such films. Thus, sub-wavelength spatial localization and sub-cycle temporal localizations are both possible simultaneously in metal-dilectric percolation films. A paper describing a theory of this novel phenomenon is published in Ref. [3.1].
2. The electromagnetic field distribution for thin metal nanowires has been theoretically calculated, by using the discrete dipole approximation. The plasmon polariton modes in wires are numerically simulated. These modes are found to be dependent on the incident light wavelength and direction of propagation. The existence of localized plasmon modes and strong local field enhancement in percolation nano-wire composites is demonstrated. Novel left-handed nanowire composite is proposed; this nanoneedle composite material may have a negative refractive index in the visible and near-infrared spectral ranges, including the telecommunication wavelength 1.5 μm. These novel metamaterials may result in developing optical lenses

that allow sub-wavelength image reconstruction and thus can act as perfect lenses. A paper describing these results is published in Ref. [3.2].

3. Direct manifestation of electron energy quantization in metal nanoparticles is observed in two-photon excited luminescence. Experiments reveal the discrete spectra in broadband anti-Stokes photoluminescence from aggregates of silver colloid particles. A theory based on spherical quantum-well model for metal nanoparticles is in good agreement with experimental observations. Preliminary results on this subject are published in Ref. [3.3]. We also submitted a paper to Physical Review Letters.
4. An analytical theory for extraordinary light transmittance through an optically thick metal film with subwavelength holes is developed. It is shown that the film transmittance has sharp peaks that are due to the Maxwell-Garnet resonances in the holes. There are localized electric and magnetic resonances resulting in, respectively, dramatically enhanced electric and magnetic fields in the holes. A simple analytical expression for the resonance transmittance is derived that holds for arbitrary hole distribution. It is also shown that there are other types of transmittance resonances, when the holes are arranged into a regular lattice. These resonances occur because of the excitation of surface plasmon polaritons propagating over the film surface. A combination of the two kinds of resonances results in a rich spectral behavior in the extraordinary optical transmittance. A paper describing this research has been published in Ref. 4.

We have also published 3 book chapters [3.5-3.7] describing some of the results outlined above.

References to Section 3

3.1 V. A. Podolskiy, A. K. Sarychev, V. M. Shalaev, "Temporal Dynamics of Local Optical Responses and Sub-fs Pulse Generation in Semicontinuous Metal Films," Laser Physics **12**, 292 (2001).

3.2 V. A. Podolskiy, A. K. Sarychev, V. M. Shalaev, Plasmon modes in metal nanowires and left-handed materials J. of Nonlinear Optical Physics and Materials **11**, #3, pp. 65-74 (2002).

3.3 V. P. Drachev, W. Kim, V. P. Safonov, V. A. Podolskiy, N. S. Zakovryazhin, V. M. Shalaev, and R. A. Armstrong, Low-threshold lasing and broad-band multiphoton-excited light emissionfrom Ag aggregate-adsorbate complexes in microcavity, J. of Modern Optics **49**, 645 (2002)

3.4 V. A. Podolskiy, A. M. Dykhne, , A. K. Sarychev, and V. M. Shalaev, Resonance Transmittance Through a Metal Film with Subwavelength Holes, IEEE J. of Quantum Electronics **38,** 956-963 (2002).

3.5 Vladimir M. Shalaev, "Optical Properties of Fractal Composites," Chapter in: *Optical Propertiesof Random Nanostructures*, Ed: Vladimir M. Shalaev, Springer Verlag, Topics in Applied Physics v.82, Berlin Heidelberg 2002.

3.6 W.T.Kim, V. P.Safonov, V. P. Drachev,V. A.Podolskiy, V. M. Shalaev, and R.L.Armstrong, "Fractal-Microcavity Composites: Giant Optical Responses," Chapter in: *Optical Properties of Random Nanostructures*, Ed: Vladimir M. Shalaev, Springer Verlag, Topics in Applied Physics, Berlin Heidelberg 2002.

3.7 A. K. Sarychev and V. M. Shalaev, "Theory of Nonlinear Optical Responses in Metal-DielectricComposites," Chapter in: *Optical Properties of Random Nanostructures*, Ed: Vladimir M. Shalaev, Springer Verlag, Topics in Applied Physics, Berlin Heidelberg 2002.

2 IMPLEMENTATION PLAN FOR THE 3RD YEAR OF THE PROJECT

1.30 During the third year of the project, will synthesize nanoscale powders of photonic materials (including laser materials). The combustion and precipitation techniques will be developed and used for that.

1.31 Starting with nanopowders produced in task 1, we will synthesize bulk ceramic samples of optical materials by pressing and sintering them in the air and in vacuum.

1.32 We will study the effect of the powder particle size on operation of neodymium random laser (based, on $NdSc_3(BO_3)_4$ powder, for example).

1.33 We will "dilute" a powder of neodymium-doped random-laser material with TiO_2, the material with high refraction index and no gain or absorption, and study the dependence on ransom laser operation on concentration of TiO_2 scatterers.

1.34 We have already demonstrated the effect of aggregate of Ag nanoparticles on the gain properties of Rhodamine 6G laser dye. In the 3rd year of the project, we will study the effect of Ag aggregate on the emission and lasing properties of powders of solid-state laser materials. Ag aggregate will be synthetized by the Purdue University team.

1.35 We will get nanoparticles of $NdSc_3(BO_3)_4$ coated with nano-layers of gold (the coating will be done in the University of Washington) and study the effect of gold on the emission and lasing properties of the neodymium doped powder.

1.36 If promising results will be demonstrated in tasks ## 4-7, we will proceed with fabrication of the bulk ceramic samples of the corresponding composite materials.

Purdue University team

1.37 Metal nanoparticles: quantum size effect, hyper-Rayleigh scattering, and saturation effects

We plan to study the energy discretization in metal quantum dots. We also plan to generalize the quantum-size effect theory and describe the saturation effects in metal nanoparticles. We will also perform experimental studies on hyper-Rayleigh scattering in silver colloid particles. The spectral dependence of Kerr-optical nonlinearity in metal dots will be investigated. We will also study the quantum size effect in nonlinear optical responses of metal dots.

1.38 Composite materials (in conjunction with task #5)

We will continue our collaborative projects with NSU on optical studies of composite materials. In particular, we plan to further study composites including fractal colloid aggregates and various lasing materials. We also plan to work on a theory for diffused reflection in ceramics.

We plan to perform spectroscopy (including nonlinear spectroscopy) studies of molecules in fractal colloid aggregates and fractal-microcavity composites.

1.39 Semicontinuous metal films

During the third year of the project, we plan to further investigate optical properties of semicontinuous metal films. Specifically, we plan to study the metal-coverage dependence of local optical responses in metal-dielectric films, using

near-field optical microscopy/spectroscopy. We will also develop a theory and numerical codes to describe the fundamental phenomenon of localization of plasmons in percolation composites.

3 PERSONNEL AND FINANCIAL REPORT

3.1 Responsibilities of the members of the NSU management and research team and evaluation of their activity

(1) Dr. Larry Mattix, PI of the project till 02.07.2002

Management of funds, resources, work loads of the faculty researchers, and student stipends.

(2) Dr. M. A. Noginov, co-PI of the project till 02.07.2002 and the P.I. of the project after 02.07.2002

Management of funds, resources, work loads of the faculty researchers, and student stipends (after 02.07.2002). Coordination of the research activities of different members of the NSU team, NASA research team, and subcontractors (Purdue University and NMSU University). Experimental and theoretical studies of stimulated emission in random lasers. Supervised students.

(3) Dr. N. Noginova, researcher

Theoretical modeling of the diffusion in random lasers

(4) Dr. L. Salary, researcher

Experimental studies of the mixtures of Rhodamine 6G dye and Aggregates of silver nanoparticles.

(5) Dr. Ed Gillman, researcher

Development of angle resolved XPS procedure for determining surface contamination (nondistrctive)

(6) Dr. G. B. Loutts, researcher (not directly supported by the project)

Synthesis of nanoperticles of optical materials and development of the ceramic synthesis technique for composite laser and nonlinear optics media.

(7) Dr. M. Bahoura, researcher (not directly supported by the project)

Experimental and theoretical studies of random lasers, supervising students.

The results of our studies have been recognized by the international research community. A number of papers have been published in the internationally circulating journals and presented at the international conferences.

(1) M. Bahoura, K. J. Morris; M. A. Noginov, "Threshold and slope efficiency of $Nd_{0.5}La_{0.5}Al_3(BO_3)_4$ ceramic random laser: effect of the pumped spot size", Optics Communications, **201**, pp. 405-412 (2002).

(2) H. J. Caulfield, D. Henderson, M. A. Noginov, "Randomness in complex media", in Complex Mediums III: Beyond Linear Isotropic Dielectrics, Akhlesh Lakhtakia, Graeme Dewar, Martin M. McCall, Editors, Proceedings of SPIE Vol. **4806**, pp. 1-17. **Invited "inaugural" lecture**

(3) M. A. Noginov, M. Bahoura, K. Morris, N. Noginova, "Random laser without diffusion?", in *OSA Trends in Optics and Photonics, (TOPS) Vol. 74, Quntum Electronics and Laser Science Conferene*, OSA Technical Digest, Postconference Edition, (Optical Society of America, Washington DC, 2002), p. 3.

(4) K. Morris, M. Bahoura, M. A. Noginov, "Random Laser based on $Nd_{0.5}La_{0.5}Al_3(BO_3)_4$ ceramic: The dependence of stimulated emission parameters on the diameter of the pumped spot", OSA Annual Meeting, Oct. 14-18, 2001, Long Beach, CA, paper #ThV2.

(5) M. A. Noginov, M. Vondrova, S. Williams, K. Sakavuyi, L. Salary, V. Drachev, "Effect of fractal Ag aggregate on spectroscopic properties of Rhodamine 6G laser dye", accepted for presentation at the OSA annual meeting, Oct. 2002, Orlando, FL.

(6) M. A. Noginov, N. Noginova, M. Bahoura, V. Drachev, "Diffused reflection off absorbing random laser material", accepted for presentation at the OSA annual meeting, Oct. 2002, Orlando, FL.

(7) M. A. Noginov, M. Bahoura, "Determination of the transport mean path in tightly packed powders of optical materials", accepted for presentation at the OSA annual meeting, Oct. 2002, Orlando, FL.

(8) M. A. Noginov, "Phase synchronization and coherent mode formation in random laser", accepted for presentation at the OSA annual meeting, Oct. 2002, Orlando, FL.

3.2 Brief financial report

3.2.1 The major expenditures in the second year of the project (spent/ encumbered)

	Amount	Purchased
Subcontracts		
Ctr for Ed Dev	100,000	10/25/01
Purdue University	20,000	6/19/02
	45,083	7/23/02
Total subcontracts	**165,083**	
Student		
Graduates/Undergrads (Summer Program 2002)	**248,667**	
Equipment		
CVI Laser Corp East	3,060	7/16/02
Hamamatsu Corp	129,000	8/13/01
Computer	1,099	12/21/01
Materials Research Furnaces	74,000	9/4/02
VA Correctional Enterprises	797	8/12/02
Newport Corp.	3,650	7/26/02
Total Equipment	**211,606**	

3.2.2 The expected carry-over funds remaining as of (projected to be spent by the end of 2002)

General Operating	40,849
Employee Benefit	16,765
Staff Salaries	11,899
Faculty Salary	2,732
Wages	18,405
Emp Dev/Transpor	7,709
Transfer Payment	15,885
Equipment	19,390
Fac & Admin	59,677
Total	**193,311**